

# **SIMULATION OF IMPACT INDUCED DETONATION OF AIM-120 A NOVEL APPROACH**

**Firooz A. Allahdadi  
David F. Medina  
Eric T. Olson  
Scott R. Jeffers**

**August 1998**

**DISTRIBUTION STATEMENT A**  
Approved for Public Release  
Distribution Unlimited

**Final Report**

**20000710 101**




**Weapons, Space, And Nuclear Safety Division  
AIR FORCE SAFETY CENTER  
KIRTLAND AIR FORCE BASE, NM 87117-5670**

---


# **Simulation of Impact Induced Detonation of AIM-120 A Novel Approach**

Air Force Safety Center  
Weapons, Space, and Nuclear Safety Division  
Kirtland AFB New Mexico

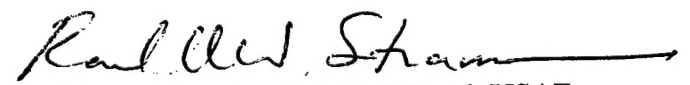
Prepared By:

  
FIROOZ A. ALLAHDADI, Ph.D.  
Chief, Numerical Simulations Engineering

Reviewed By:

  
CATHERINE J. ZERINGUE, LtCol, USAF  
Chief, Space & Engineering Branch

Approved By:

  
RANDALL W. STRAUSS, Colonel, USAF  
Chief, Weapons, Space, and Nuclear Safety Division

10 March 2000

REPORT DOCUMENTATION PAGE			Form Approved OMB No. 0704-0188	
<small>Public reporting burden for this collection of information is estimated to average 1 hour per response, including the time for reviewing instructions, searching existing data sources, gathering and maintaining the data needed, and completing and reviewing the collection of information. Send comments regarding this burden estimate or any other aspect of this collection of information, including suggestions for reducing this burden, to Washington Headquarters Services, Directorate for Information Operations and Reports, 1215 Jefferson Davis Highway, Suite 1204, Arlington, VA 22202-4302, and to the Office of Management and Budget, Paperwork Reduction Project (0704-0188), Washington, DC 20503.</small>				
1. AGENCY USE ONLY (Leave blank)		2. REPORT DATE March 2000		3. REPORT TYPE AND DATES COVERED Final Report
4. TITLE AND SUBTITLE Simulation of Impact Induced Detonation of AIM-120 A Novel Approach			5. FUNDING NUMBERS N/A	
6. AUTHOR(S) Firooz A. Allahdadi, David F. Medina, Eric T. Olson, Scott R. Jeffers				
7. PERFORMING ORGANIZATION NAME(S) AND ADDRESS(ES) Air Force Safety Center/SEWE 9700 G Avenue, SE Kirtland AFB, NM 87117-5670			8. PERFORMING ORGANIZATION REPORT NUMBER  AFSC-TR-2000-0002	
9. SPONSORING/MONITORING AGENCY NAME(S) AND ADDRESS(ES)			10. SPONSORING/MONITORING AGENCY REPORT NUMBER	
11. SUPPLEMENTARY NOTES				
12a. DISTRIBUTION AVAILABILITY STATEMENT Approved for public release; distribution is unlimited.			12b. DISTRIBUTION CODE	
13. ABSTRACT (Maximum 200 words) A high fidelity computational campaign was initiated to predict impact-induced detonation. The intent of this numerical simulation campaign is to capture dynamics and the intervening physical processes leading to detonation of AIM-120 Advanced Medium Range Air-to-Air Missile (AMRAAM) warhead (WDU-33/B) resulting from fragment impact. A new and innovative first principle calculational tool called "Smoothed Particle Hydrodynamics" (SPH) is used. SPH is an unstructured free Lagrangian hydrodynamic tool developed earlier [1,2,3] for predicting consequences of high strain rate reaction processes where materials experience extreme density gradients and undergo large plastic deformation. Examples of such impulsive interactions can be found in penetration and fracture/fragmentation mechanics problems.  Well-controlled field tests are conducted to verify the detonability of the AIM-120 class missile warheads to high-speed fragment impacts. Detailed temporally and spatially varying fragment impact calculations are performed to illustrate the response of the AIM-120 to the kinetic energy of the impinging fragments. The correlation between calculational predictions and the field tests data are presented.				
14. SUBJECT TERMS modeling, computational numerical simulation, impact-induced detonation, AMRAAM, warhead WDU-33/B, fragment impact, AIM-120			15. NUMBER OF PAGES 34	
			16. PRICE CODE	
17. SECURITY CLASSIFICATION OF REPORT Unclassified	18. SECURITY CLASSIFICATION OF THIS PAGE Unclassified	19. SECURITY CLASSIFICATION OF ABSTRACT Unclassified	20. LIMITATION OF ABSTRACT	

## GENERAL INSTRUCTIONS FOR COMPLETING SF 298

The Report Documentation Page (RDP) is used in announcing and cataloging reports. It is important that this information be consistent with the rest of the report, particularly the cover and title page. Instructions for filling in each block of the form follow. It is important to **stay within the lines** to meet **optical scanning requirements**.

**Block 1. Agency Use Only (Leave blank).**

**Block 2. Report Date.** Full publication date including day, month, and year, if available  
(e.g. 1 Jan 88). Must cite at least the year.

**Block 3. Type of Report and Dates Covered.** State whether report is interim, final, etc. If applicable, enter inclusive report dates (e.g. 10 Jun 87 - 30 Jun 88).

**Block 4. Title and Subtitle.** A title is taken from the part of the report that provides the most meaningful and complete information. When a report is prepared in more than one volume, repeat the primary title, add volume number, and include subtitle for the specific volume. On classified documents enter the title classification in parentheses.

**Block 5. Funding Numbers.** To include contract and grant numbers; may include program element number(s), project number(s), task number(s), and work unit number(s). Use the following labels:

C - Contract  
G - Grant  
PE - Program  
Element

PR - Project  
TA - Task  
WU - Work Unit  
Accession No.

**Block 6. Author(s).** Name(s) of person(s) responsible for writing the report, performing the research, or credited with the content of the report. If editor or compiler, this should follow the name(s).

**Block 7. Performing Organization Name(s) and Address(es).**  
Self-explanatory.

**Block 8. Performing Organization Report Number.** Enter the unique alphanumeric report number(s) assigned by the organization performing the report.

**Block 9. Sponsoring/Monitoring Agency Name(s) and Address(es).**  
Self-explanatory.

**Block 10. Sponsoring/Monitoring Agency Report Number.** (If known)

**Block 11. Supplementary Notes.** Enter information not included elsewhere such as: Prepared in cooperation with....; Trans. of....; To be published in.... When a report is revised, include a statement whether the new report supersedes or supplements the older report.

**Block 12a. Distribution/Availability Statement.** Denotes public availability or limitations. Cite any availability to the public. Enter additional limitations or special markings in all capitals (e.g. NOFORN, REL, ITAR).

**DOD** - See DoDD 5230.24, "Distribution Statements on Technical Documents."

**DOE** - See authorities.

**NASA** - See Handbook NHB 2200.2.

**NTIS** - Leave blank.

**Block 12b. Distribution Code.**

**DOD** - Leave blank.

**DOE** - Enter DOE distribution categories from the Standard Distribution for Unclassified Scientific and Technical Reports.

Leave blank.

**NASA** - Leave blank.

**NTIS** -

**Block 13. Abstract.** Include a brief (*Maximum 200 words*) factual summary of the most significant information contained in the report.

**Block 14. Subject Terms.** Keywords or phrases identifying major subjects in the report.

**Block 15. Number of Pages.** Enter the total number of pages.

**Block 16. Price Code.** Enter appropriate price code (*NTIS only*).

**Blocks 17. - 19. Security Classifications.** Self-explanatory. Enter U.S. Security Classification in accordance with U.S. Security Regulations (i.e., UNCLASSIFIED). If form contains classified information, stamp classification on the top and bottom of the page.

**Block 20. Limitation of Abstract.** This block must be completed to assign a limitation to the abstract. Enter either UL (unlimited) or SAR (same as report). An entry in this block is necessary if the abstract is to be limited. If blank, the abstract is assumed to be unlimited.

## TABLE OF CONTENTS

<b>TABLE OF CONTENTS</b> .....	<b>i</b>
<b>List of Figures</b> .....	<b>ii</b>
<b>List of Tables</b> .....	<b>iii</b>
<b>Acknowledgments</b> .....	<b>iv</b>
<b>Abstract</b> .....	<b>1</b>
<b>Introduction</b> .....	<b>1</b>
<b>Theoretical Development</b> .....	<b>1</b>
1. The Kernel, Smoothing Function.....	3
2. SPH Formulation of Hydrodynamics Equations.....	3
3. Constitutive Relations.....	4
4. Artificial Viscosity.....	5
<b>Numerical Simulation</b> .....	<b>5</b>
1. AMRAAM Warhead Geometry Setup†.....	6
2. Explosive Reaction Simulation.....	8
<b>Simulation Results</b> .....	<b>9</b>
1. Diagnostic Calculations.....	9
2. Five Inch Standoff Results.....	13
3. 33.5 Inch Standoff Calculation.....	17
<b>Experimental Effort</b> .....	<b>22</b>
1. Test Plan.....	22
<b>Conclusions</b> .....	<b>23</b>
<b>References</b> .....	<b>24</b>

## List of Figures

Figure 1. WDU-33/B Warhead model. ....	7
Figure 2. Problem setup parameters. ....	7
Figure 3. Two Dimensional model. ....	10
Figure 4. Rupture characteristics of the WDU-33/B Warhead. ....	11
Figure 5. Fragment velocity versus time. ....	11
Figure 6. Two-dimensional calculation of the WDU-33/B casing being impacted with a warhead fragment at (a) 3608 ft/s and (b) 3973 ft/s. ....	13
Figure 7. Dimensions of a single, undeformed fragment in the WDU-33/B warhead. ....	13
Figure 8. Early time explosive expansion of the donor warhead. ....	14
Figure 9. Two-dimensional slice showing evolution of the donor warhead expansion. ....	15
Figure 10. Pressure state of acceptor warhead at incipient detonation. ....	15
Figure 11. Case expansion shortly after impact (110 microseconds). ....	16
Figure 12. Acceptor casing damage for 5 inch standoff distance at 120 microseconds. ....	16
Figure 13. Acceptor casing showing explosive expansion for 5 inch standoff at 140 $\mu$ sec. ....	17
Figure 14. F-16 wing mounted AIM-120s. ....	17
Figure 15. Progression of impacting fragments on the acceptor warhead with a 33.5 inch standoff. ....	18
Figure 16. Radial distribution of fragments at impact for the 33.5 inch standoff. ....	19
Figure 17. Fragment evolution for the 33.5 inch standoff simulation. ....	19
Figure 18. Pressure contours (kbar) in the acceptor warhead at (a) 530, (b) 540, and (c) 550 microseconds. ....	20
Figure 19. Acceptor warhead at 510 $\mu$ sec for a standoff distance of 33.5 inches. ....	20
Figure 20. Acceptor warhead at 570 $\mu$ sec showing explosive expansion. ....	21

Figure 21. Damage to acceptor casing at the start of induced detonation (540 microseconds)...21

### **List of Tables**

TABLE 1. PBX (AF)-108 EQUATION OF STATE PARAMETERS. ....	8
TABLE 2. JWL PARAMETERS FOR PBX (AF)-108. ....	8
TABLE 3. RELEVANT VALUES IN MAGI CONSTANT FILE. ....	9

## **Acknowledgments**

The authors gratefully acknowledge Mr. Paul Price for technical support and continued encouragement.



## Abstract

A high fidelity computational campaign was initiated to predict impact-induced detonation. The intent of this numerical simulation campaign is to capture dynamics and the intervening physical processes leading to detonation of AIM-120 Advanced Medium Range Air-to-Air Missile (AMRAAM) warhead (WDU-33/B) resulting from fragment impact. A new and innovative first principle calculational tool called "Smoothed Particle Hydrodynamics" (SPH) is used. SPH is an unstructured free Lagrangian hydrodynamic tool developed earlier [1,2,3] for predicting consequences of high strain rate reaction processes where materials experience extreme density gradients and undergo large plastic deformation. Examples of such impulsive interactions can be found in penetration and fracture/fragmentation mechanics problems.

Well-controlled field tests are conducted to verify the detonability of the AIM-120 class missile warheads to high-speed fragment impacts. Detailed temporally and spatially varying fragment impact calculations are performed to illustrate the response of the AIM-120 to the kinetic energy of the impinging fragments. The correlation between calculational predictions and the field tests data are presented.

## Introduction

A unique alternative to conventionally used structured Lagrangian or Eulerian analytical tools in computational fluid dynamics is Smoothed Particle Hydrodynamics (SPH). The SPH method is an unstructured, grid-free, Lagrangian scheme used to solve a wide range of problems in continuum mechanics and fluid dynamics. This computational method simulates the motion of a continuous medium by representing the medium as an interacting finite system of moving particles. This method employs no grid, therefore it avoids any grid distortion problems, which occur in other Lagrangian techniques when calculating large density gradients and deformations. The principle of SPH was first developed and introduced as a viable alternative to the commonly used structured Lagrangian method by Lucy [4], Gingold[5-7], Monaghan [8,9], and Benz [10].

The basis of SPH lies in the interpolation procedure where all thermodynamic field variables (density, pressure, and internal energy) are evaluated at the discrete set of points (particles). These points are arbitrary and randomly distributed in space. The interpolation procedure uses an interpolating kernel function to approximate any function of position as an integral transformation. Using integration by parts, the integral transformation of spatial derivatives of functions can be re-expressed as integral transformations of the function itself. These integral interpolants are approximated by sums over a finite number of particle positions or points. The summation interpolant then replaces the governing partial differential equations of continuum mechanics with a set of ordinary equations.

## Theoretical development

The principles of Smoothed Particle Hydrodynamics that were introduced above will now be further described and developed. By definition, the SPH method is based on the motion of a finite number of interacting material particles distributed randomly in space. Each variable of the continuum field in SPH,  $f(\vec{r})$ , is approximated by an integral interpolant  $\langle f(\vec{r}) \rangle$  given by

$$\langle f(\vec{r}) \rangle = \int f(\vec{r}') W(|\vec{r} - \vec{r}'|, h) d\vec{r}', \quad (1)$$

which will be replaced by a sum over the particle positions.

The function  $W$  is the smoothing or interpolation function (kernel) and has a width measured by  $h$  called smoothing length. For all positive kernels, i.e.  $W > 0$ , the smoothing function can be normalized to unity.

$$\int W(|\vec{r}|, h) d\vec{r} = 1 \quad (2)$$

and it follows that  $\langle f(\vec{r}) \rangle \rightarrow f(\vec{r})$  as  $h \rightarrow 0$ .

The mathematical expression described in (1) therefore defines the kernel estimate (integral interpolant)  $\langle f \rangle$  of  $f$ . It is important to note that the smoothing function  $W$  resembles the properties of Dirac delta function when  $h \rightarrow 0$ .

Suppose the function  $f(\vec{r})$  is known only at  $N$  discrete points (the particle positions  $\vec{r}_1, \vec{r}_2, \dots$ ), i.e., they are spatially distributed according to the number density distribution,  $\eta(\vec{r})$

$$\eta(\vec{r}) = \sum_{j=1}^N \delta(\vec{r} - \vec{r}_j). \quad (3)$$

Now if we associate with the  $j$ -th particle a volume,

$$dr' = \frac{m_j}{\rho(\vec{r}_j)} \quad (4)$$

we may then approximate the integral interpolant in Equation 1 with the following sum over the particle positions:

$$\langle f(\vec{r}) \rangle \cong \sum_{j=1}^N f(\vec{r}_j) W(|\vec{r} - \vec{r}_j|, h) \frac{m_j}{\rho_j} \quad (5)$$

where  $\rho_j = \rho(\vec{r}_j)$ .

The approximation methodology described above will permit us to conveniently estimate the dynamic and thermodynamic quantities of motion as described by the Navier-Stokes Equations and constitutive models. Now in the case where  $f(\vec{r})$  is replaced by the density  $\rho(\vec{r})$ , then Equation 5 becomes,

$$\langle \rho(\vec{r}) \rangle = \sum_{j=1}^N m_j W(|\vec{r} - \vec{r}_j|, h) \quad (6)$$

Equation 6 has a fundamental physical interpretation: it states that every material particle has a mass which is smoothed out in space in accordance with the specific smoothing function  $W$  and smoothing length  $h$ . Therefore, density of the medium can be defined as a sum of the density distributions of all the particles in the vicinity of the specific point.

## 1. The Kernel, Smoothing Function

There are two interpolation kernels or smoothing functions most commonly used in SPH. They are Gauss kernel and Cubic B-Spline kernel. For more detailed discussion see References 11 and 12.

## 2. SPH Formulation of Hydrodynamics Equations

We use the conservation equations of continuum mechanics in the form:

CONSERVATION OF MASS

$$\frac{d\rho}{dt} = -\rho \vec{\nabla} \cdot \vec{V} \quad (7)$$

CONSERVATION OF MOMENTUM

$$\frac{dV^\alpha}{dt} = -\frac{1}{\rho} \nabla^\beta \sigma^{\alpha\beta} \quad (8)$$

CONSERVATION OF ENERGY

$$\frac{dE}{dt} = -\frac{\sigma^{\alpha\beta}}{\rho} \nabla^\beta V^\alpha \quad (9)$$

Dependent variables are the scalar density ( $\rho$ ) and the specific internal energy ( $E$ ), the velocity vector ( $\vec{V}$ ), and the stress tensor  $\sigma^{\alpha\beta}$ . The independent variables are the spatial coordinates  $X^\alpha$  and the temporal variable  $t$ . Here the total time derivative ( $d/dt$ ) is taken in the moving Lagrangian frame. Summation over repeated Greek indices are implied. Using Equation 5, the governing hydrodynamic equations are approximated in the SPH framework. They become:

CONSERVATION OF MASS

$$\frac{d\rho_i}{dt} = \sum_j m_j (\vec{V}_i - \vec{V}_j) \cdot \vec{\nabla}_i W(\vec{r}_i - \vec{r}_j, h) \quad (10)$$

### CONSERVATION OF MOMENTUM

$$\frac{dV_i^\alpha}{dt} = - \sum_j m_j \left( \frac{\sigma_i^{\alpha\beta}}{\rho_i^2} + \frac{\sigma_j^{\alpha\beta}}{\rho_j^2} \right) \nabla_i^\beta W(|\vec{r}_i - \vec{r}_j|, h) \quad (11)$$

### CONSERVATION OF ENERGY

$$\frac{dE_i}{dt} = \frac{\sigma_i^{\alpha\beta}}{\rho_i^2} \sum_j m_j (V_i^\alpha - V_j^\alpha) \nabla_i^\beta W(|\vec{r}_i - \vec{r}_j|, h) \quad (12)$$

It should be noted that an alternative form of conservation of mass equation can be obtained from Equation 6. It reads

$$\rho_i = \sum_j m_j W(|\vec{r}_i - \vec{r}_j|, h) \quad (13)$$

### 3. Constitutive Relations

The stress tensor appearing in the momentum and energy Equations 11 and 12, respectively, is decomposed into an isotropic part which is the pressure ( $P$ ) and the traceless symmetric deviatoric stress tensor  $S^{\alpha\beta}$

$$\sigma^{\alpha\beta} = P \delta^{\alpha\beta} - S^{\alpha\beta} \quad (14)$$

The pressure term is calculated by means of the equation of state in the form  $P = p(\rho, E)$  such as the Mie Gruneisen equation for solids or Gamma -Law for the gases. The two respective equations are:

Mie Gruneisen,

$$\begin{aligned} P(\rho, E) &= (1 - 0.5\Gamma\eta) P_H(\rho) + \Gamma \rho E \\ P_H &= a_0 \eta + b_0 \eta^2 + c_0 \eta^3 \quad \eta > 0 \\ P_H &= a_0 \eta \quad \eta < 0 \end{aligned} \quad (15)$$

Ideal Gas Law,

$$P = (\gamma - 1) \rho E \quad (16)$$

The subscript "H" refers to the Hugoniot curve, while  $\eta = \rho / \rho_0 - 1$  represents the compression and  $\Gamma$  is the Gruneisen parameter. The constants  $a_0$ ,  $b_0$ , and  $c_0$  in Equation 15 are related to the coefficients  $C$  and  $S$  in the shock and particle velocity relation  $U_s = C + S U_p$  through a Taylor's series expansion of the Hugoniot curve  $P_H$ . The ratio of heat capacities at constant pressure and constant volume respectively is represented by  $\gamma = C_p / C_v$ .

The anisotropic part of the stress tensor can be written in a variety of forms [13,14]. For application in SPH, the deviatoric stress field, assuming small displacement, can be written as

$$\dot{S}^{\alpha\beta} = \mu \bar{\epsilon}^{\alpha\beta} = \mu \left( \dot{\epsilon}^{\alpha\beta} - \frac{1}{3} \delta^{\alpha\beta} \dot{\epsilon}^{\gamma\gamma} \right) \quad (17)$$

where  $\mu$  is the shear modulus and  $\dot{\epsilon}$  is the strain rate.

#### 4. Artificial Viscosity

To numerically resolve sharp gradients and steep variation of the physical parameters at the shock front, the concept of artificial viscosity is introduced. The artificial viscosity function smoothes and smears the shock front over a few resolution lengths. This concept was first introduced by Von Neumann and Richtmyer [15]. A special form of the artificial viscosity function for use in SPH was developed by Monaghan and Gingold [7]. It has the following form:

$$\begin{aligned} \Pi_{ij} &= \frac{-\alpha \bar{C}_{ij} \omega_{ij} + \beta \omega_{ij}^2}{\bar{\rho}_{ij}}, & (\vec{V}_i - \vec{V}_j) \cdot (\vec{r}_i - \vec{r}_j) < 0; \\ \Pi_{ij} &= 0, & (\vec{V}_i - \vec{V}_j) \cdot (\vec{r}_i - \vec{r}_j) > 0. \end{aligned} \quad (18)$$

where

$$\begin{aligned} \omega_{ij} &= \frac{h (\vec{V}_i - \vec{V}_j) \cdot (\vec{r}_i - \vec{r}_j)}{(\vec{r}_i - \vec{r}_j)^2 + \epsilon h^2}, & \alpha \approx 1.0, \beta \approx 2.0, \epsilon \approx 0.01 \\ \bar{\rho}_{ij} &= \frac{1}{2} (\rho_i + \rho_j), \bar{C} = \frac{1}{2} (C_i + C_j) \end{aligned}$$

Here the quantity  $C$  is the speed of sound.

### Numerical Simulation

Detonability of AIM-120 warhead to fragment impact is simulated in three dimensions using the Smoothed Particle Hydrodynamics (SPH) method described in section III. Broadly speaking, there are two independent however interrelated sequential phases to this numerical simulation. Each phase is simulated in a continuous numerical process which applies fundamental physics to assess the complex interactions between the two phases. The first phase of simulation consists of detonation, breakup and fragmentation of the AIM-120 donor warhead. The importance of solving the donor explosion from a first principles foundation is apparent. One must accurately characterize fragment shape and distribution, incident impact angle, and impact speed before predicting failure modes (i.e., detonability) of the warhead acceptor. In this simulation some effects such as fragment distortion, inter-fragment distance, rotation, or skewness are considered second order effects and are ignored.

Next, propagation of the radially expanding fragments is modeled and tracked both spatially and temporally before they impact a second AIM-120 warhead, referred to as the acceptor warhead. The acceptor warhead is positioned at a specified configuration and at a prescribed standoff distance with respect to the donor warhead. The second phase of the simulation consists of determining the response of the warhead acceptor to the kinetic energy of the impacting donor fragments. The complex phenomena involved in the impact process, including possible perforation of the warhead casing and the ensuing shock loading of the PBX (AF)-108 explosive, is simulated at this stage. Finally, the induced pressure level in the acceptor warhead is assessed to determine whether it exceeds the threshold value required for sustaining a detonation. The threshold pressure value necessary for initiating a self-sustaining detonation front in PBX (AF)-108 is estimated to be 20 kbar.

### 1. AMRAAM Warhead Geometry Setup<sup>†</sup>

The physical geometry of the donor and acceptor warheads is constructed (generated) in three dimensions using the SPH code *MAGI*. The AISI-4140 medium carbon-chromium steel used in the warhead casing is modeled by the Mie-Gruneisen Equation of State and the Elastic-Perfectly-Plastic constitutive strength model. Special coding was developed to construct interior and exterior scoring of the warhead casing. To capture dynamics of the case rupture along the score lines and fragmentation, the Johnson and Cook fracture model [16] was used. The Johnson-Cook fracture model uses a failure criteria based on equivalent plastic strain, taking into account the pressure, temperature, and strain rate along the loading path for each material element. The warhead model with the explosive removed is shown in Figure 1. The hanger assembly shown in this figure was placed in the model in anticipation of assessing the resulting fragment distribution and its effect on an acceptor warhead. For the simulations reported here, the hanger was oriented away from the acceptor warhead. Further specifics of the warhead geometry and problem setup are given in Figure 2. This 3-D model was constructed from warhead engineering drawings and used 909,578 particles resulting in a resolution of 1.7 mm (particle diameter) in the acceptor explosive material and the donor and acceptor casing. This resolution was verified in a 2-D convergence analysis described later. The 3-D simulation used two reflective planes of symmetry along the donor and acceptor warhead. The simulations were executed on a shared memory parallel machine and required about 1000 cpu hours among 16 processors.

---

<sup>†</sup> calculations are performed by Mr. David Medina at AFRL/DEPA.

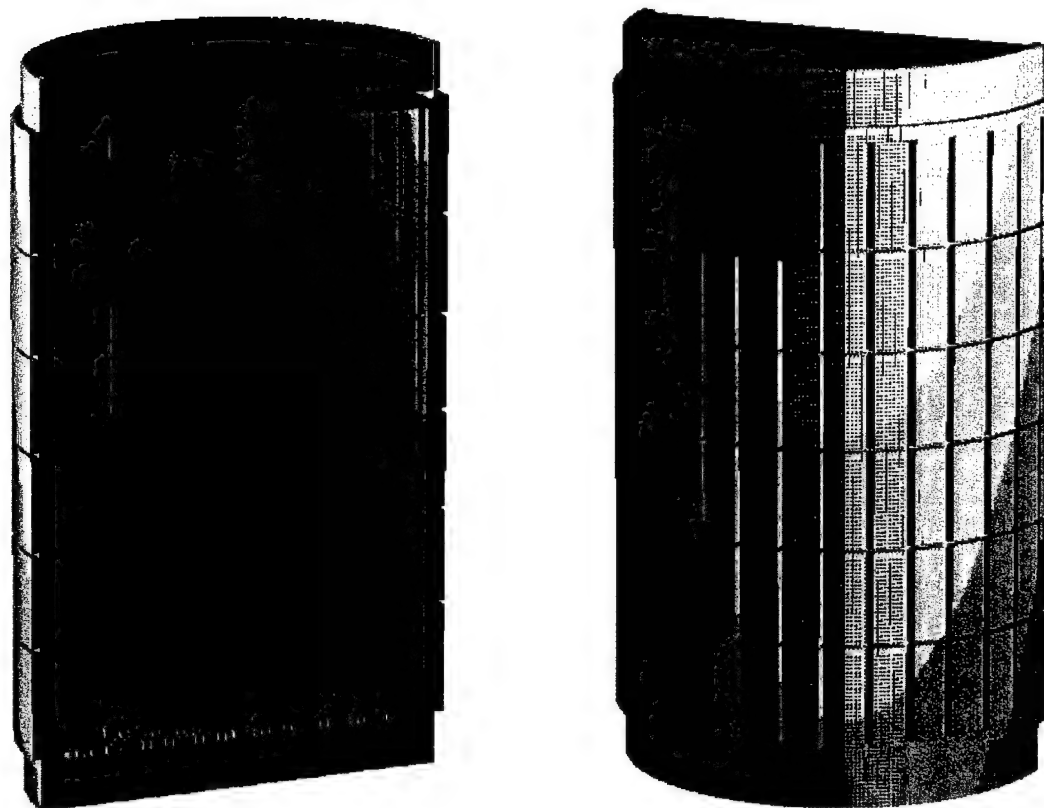


Figure 1. WDU-33/B Warhead model.

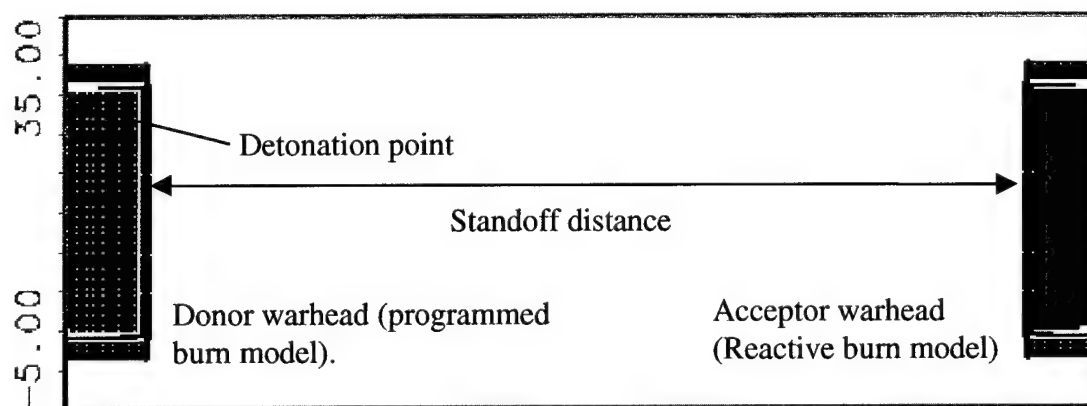


Figure 2. Problem setup parameters.

## 2. Explosive Reaction Simulation

A total of 6783 grams equivalent PBX (AF)-108 explosive was used in the simulation of the AMRAAM (AIM-120) warhead (WDU-33/B). It is important to note that the 6783 grams PBX used in the simulation consisted of two parts; 6652 grams main charge plus 131 grams equivalent PBX to account for the 110 grams of CH-6 explosive used in the warhead booster. This energy equivalent conversion is based on a 1.189 conversion factor obtained from the ratio of mass density of RDX used in CH-6 to that of PBX.

The unreacted solid explosive used in these simulations was represented by the Mie-Gruneisen equation of state. The gas phase of the reacted explosive was modeled with the JWL equation of state (EOS). The JWL EOS describes the pressure, volume, and energy relationships in the adiabatic expansion region of the explosive products, given by

$$P = A \left[ 1 - \frac{\omega}{R_1 V} \right] e^{-R_1 V} + B \left[ 1 - \frac{\omega}{R_2 V} \right] e^{-R_2 V} + \frac{\omega E}{V} \quad (19)$$

For isentropic processes, the pressure ( $P_s$ ) is,

$$P_s = A e^{-R_1 V} + B e^{-R_2 V} + C V^{-(\omega+1)} \quad (20)$$

where  $P$  is the pressure of the detonation products,  $A$ ,  $B$ , and  $C$  are linear coefficients,  $R_1$ ,  $R_2$ , and  $\omega$  are nonlinear coefficients,  $V$  is the ratio of the detonation products volume ( $v$ ) to the initial explosive volume ( $v_0$ ), and  $E$  is the detonation energy per unit volume.

The physical constants specific to PBX (AF)-108 were obtained from References 18,19, and 20. These values are summarized in Tables 1 and 2. Other relevant input data to the MAGI constants file is given in Table 3. It should be noted that the detonation threshold (item 78 in constants file) was obtained from Wagenhals [21].

**TABLE 1. PBX (AF)-108 EQUATION OF STATE PARAMETERS.**

Density (g/cm <sup>3</sup> )	Dv (cm/μsec)	E <sub>19</sub> (kJ/g)	P <sub>cj</sub> (kbar)	Gamma γ	ΔH <sub>det</sub> (Mbar-cc/g)
<b>1.57</b>	<b>0.791</b>	<b>1.095</b>	<b>260</b>	<b>2.784</b>	<b>0.0453</b>

**TABLE 2. JWL PARAMETERS FOR PBX (AF)-108.**

V <sub>ch</sub>	R1	R2	ω	A(Mbar)	B(Mbar)	C(Mbar)
<b>0.7358</b>	<b>4.12</b>	<b>1.031</b>	<b>0.3</b>	<b>4.725</b>	<b>0.03230</b>	<b>0.01179</b>



The Forest Fire Reactive burn model is used to calculate the incipient detonation in the acceptor warhead. In this reactive burn model, the results of simple small-scale wedge tests are applied to calibrate the model, allowing one to extrapolate to complex problems involving shock-initiated reaction of heterogeneous solid explosives. The derivation of this method is based on the assumption of a global reaction rate model for the decomposition of the explosive. The model has been successfully applied to a variety of very practical problems. For a detailed derivation, the reader is referred to Mader [22].

**TABLE 3. RELEVANT VALUES IN MAGI CONSTANT FILE.**

afx		! pbx (af)-108
1	1.6500E-01	co - ambient sound speed (cm/us) Navy Expl HB, Pg 4-24
2	1.9600E+00	s - slope of us - up line Navy Expl HB, Pg 4-28
11	1.5000E+00	Gamma - Gruneisen constant
12	2.5795E-01	Cv - specific heat (cal/(g-K) Navy Expl HB, Pg 4-33
13	6.3776E-01	Vo - ambient specific volume (cm**3) Navy Expl HB, Pg 1-5
14	7.0000E-05	alpha - coefficient of linear expansion, Navy Expl HB, Pg 4-35
15	2.5000E-01	mu - shear modulus (mb)
16	3.0000E-03	Yo - yield strength (mb)
17	3.0000E+02	To - ambient temp (K)
18	2.5000E+03	Tmelt - melt temp (K)
19	-7.0300E-06	Pmin - spall strength (mb) Navy Expl HB, Pg 5-11
20	2.0000E-02	Multiplier for density clip
68	2.2213E+02	mw - molecular weight for RDX (72% AFX) NEH Pg 2-8
69	2.7848E+00	gamma - specific heat ratio
70	4.7250E+00	jwl a - Eglin Energetic Materials Branch
71	3.2300E-02	jwl b - Eglin Energetic Materials Branch
72	1.1790E-02	jwl c - Eglin Energetic Materials Branch
73	4.1240E+00	jwl r1 - Eglin Energetic Materials Branch
74	1.0310E+00	jwl r2 - Eglin Energetic Materials Branch
75	3.0000E-01	jwl w - Eglin Energetic Materials Branch
76	7.9170E-01	detonation velocity - cm/us
77	4.5384E-02	detonation energy - mb-cc/gm Eglin Energetic Mat
78	1.8000E-02	detonation threshold for burn 2 (currently mb)
79	2.6000E-01	Chapman-Jouguet detonation pressure, From Eglin

## Simulation Results

The susceptibility of the AMRAAM (AIM-120) warhead to fragment impacts resulting in possible sympathetic detonation was simulated for two distinct standoff distances. The donor and the acceptor warheads were located at 5 and 33.5 inches standoff distances from each other in a perfect center-to-center alignment configuration. Following propagation of the donor warhead fragmentation, it becomes apparent that the likelihood of perfect normal impact on the acceptor warhead decreases with increasing cylindrical expansion of the fragments (Figure 18). The current 3-D simulations take this expansion into account over the calculational process.

### 1. Diagnostic Calculations

A set of preliminary calculations were conducted to evaluate the properties of the various physical modules. Additionally, attempts were made to assess the convergence of the results as a function of the resolution particle size and setup. A 2-Dimensional Cartesian coordinates model, shown in Figure 3, was used to model strip fragment generation and its propagation.

The smallest size fragment allowed in this analysis was a fragment formed by the scoring pattern, i.e.,  $14.8 \times 11.7 \text{ mm}^2$ .

To ensure that the scored casing was rupturing properly and the brittle fracture module behaved realistically, we compared our calculated rupture radius with the predicted rupture radius, for an unscored casing, obtained from the Gurney Equation, reference 23. As expected, the calculated scored casing rupture occurs at a reasonable time before the unscored rupture (Figure 4).

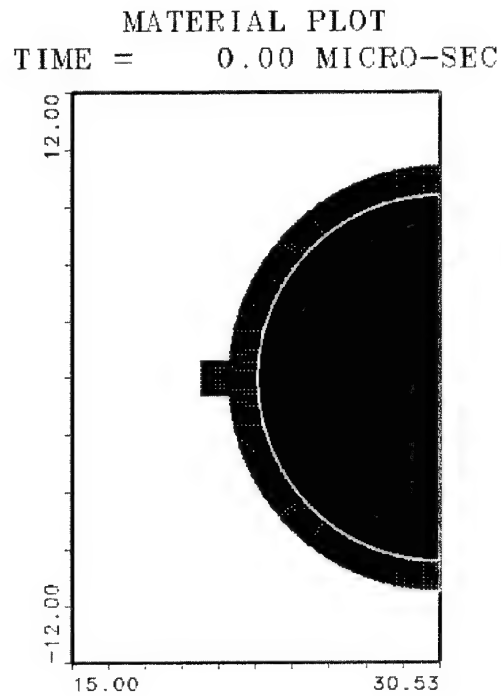


Figure 3. Two Dimensional Model.

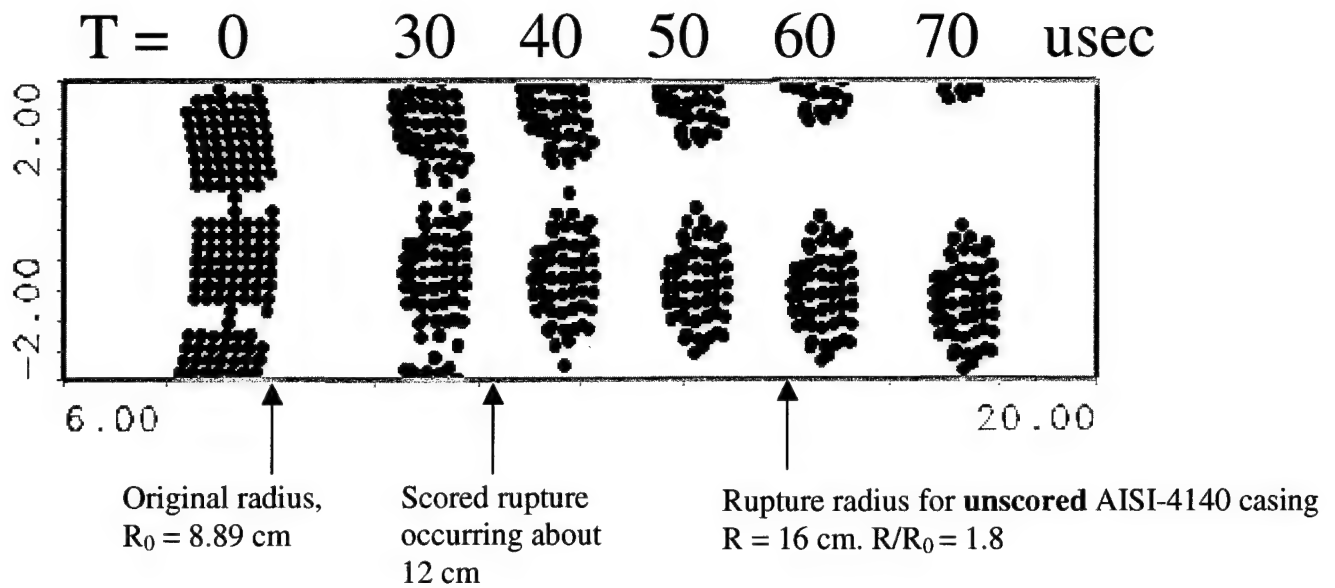


Figure 4. Rupture characteristics of the WDU-33/B Warhead.

Furthermore, the acceleration and the deceleration character of the donor fragments were assessed separately using a 2-D analysis. In this analysis, it was assumed that all the aerodynamic forces including drag and friction forces were negligible. The 2-Dimensional calculation showed that fragments reach a steady-state velocity at about 90 microseconds (Figure 5).

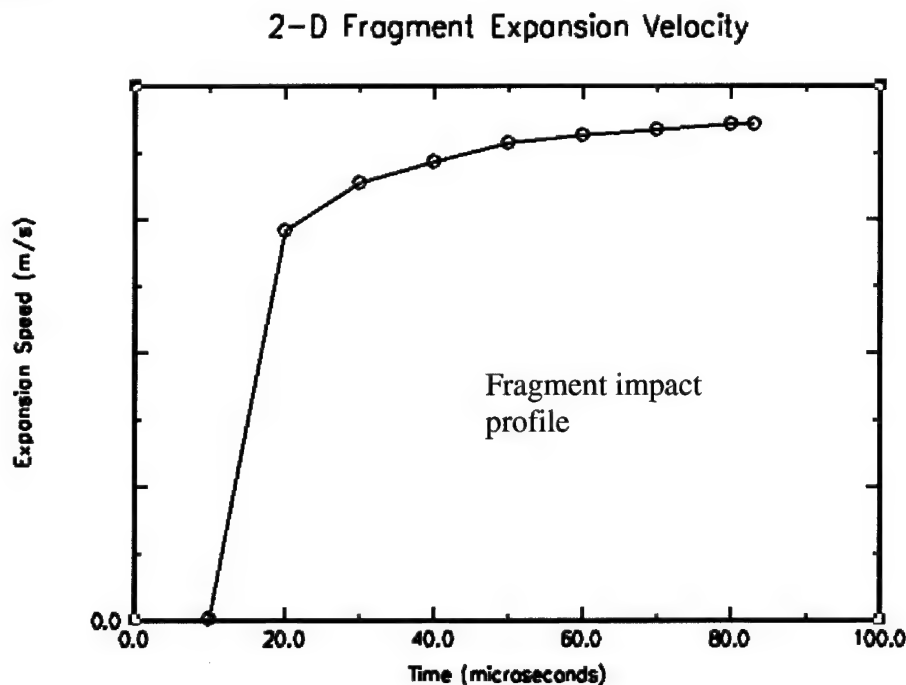


Figure 5. Fragment velocity versus time.

It is worth noting that a threshold impact velocity for detonation was established. The lower bound of impact velocity, which did not detonate, was 3608 ft/s while the upper bound, which resulted in detonation, was 3973 ft/s (Figure 6).

Finally, the threshold impact velocity for a single WDU-33/B fragment impacting the same warhead was calculated using the Jacobs-Roslund empirical formula

$$V_c = (A/d^{1/2})(1+B)(1+CT/d) \quad (21)$$

where

- $V_c$  = critical impact velocity for target detonation
- $d$  = fragment critical dimension, e.g. diameter (mm)
- $T$  = target cover thickness (mm)
- $A$  = explosive sensitivity coefficient ( $\text{mm}^{3/2}/\mu\text{sec}$ )
- $B$  = fragment shape coefficient (dimensionless)  
 $B = 0$  for flat-end fragments
- $C$  = cover plate protection coefficient (dimensionless)

The values used for PBX (AF)-108 for  $A$ ,  $B$ , and  $C$  are given in the Navy Explosives Handbook [24]. From this formula, the threshold velocity for a WDU-33/B fragment impacting the same warhead is 6876 ft/s.

There is a tight connection between the physical size of the impacting fragments, failure, or critical diameter of the explosive and the computational resolution. The critical explosive diameter is the minimum diameter at which a cylindrical charge of HE sustains a high order detonation. Although there exists adequate information on critical diameter of RDX based explosive, none was found for PBX (AF)-108 in References 24 or 25.

As shown in Figure 7, the individual fragment size in the WDU-33/B Warhead follows the scoring dimensions and is most likely well above the critical diameter of the PBX (AF)-108 explosive. Therefore, to ensure high resolution, a computational (SPH) particle size of 1.67 mm was selected for this class of impact induced detonation problem.

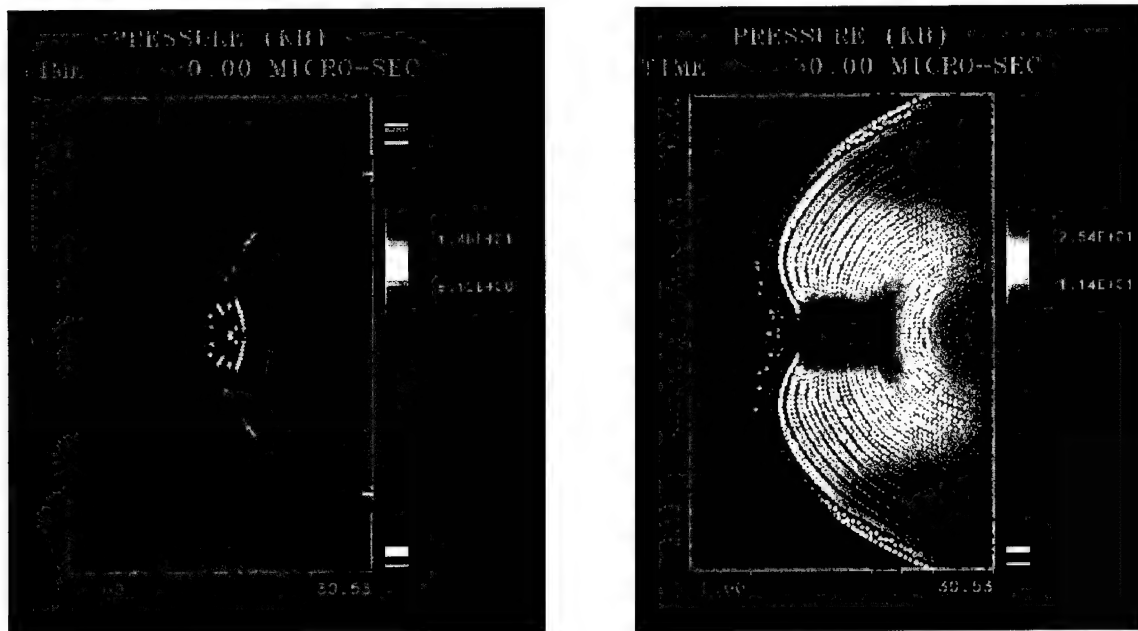


Figure 6. Two-dimensional calculation of the WDU-33/B casing being impacted with a warhead fragment at (a) 3608 ft/s and (b) 3973 ft/s.

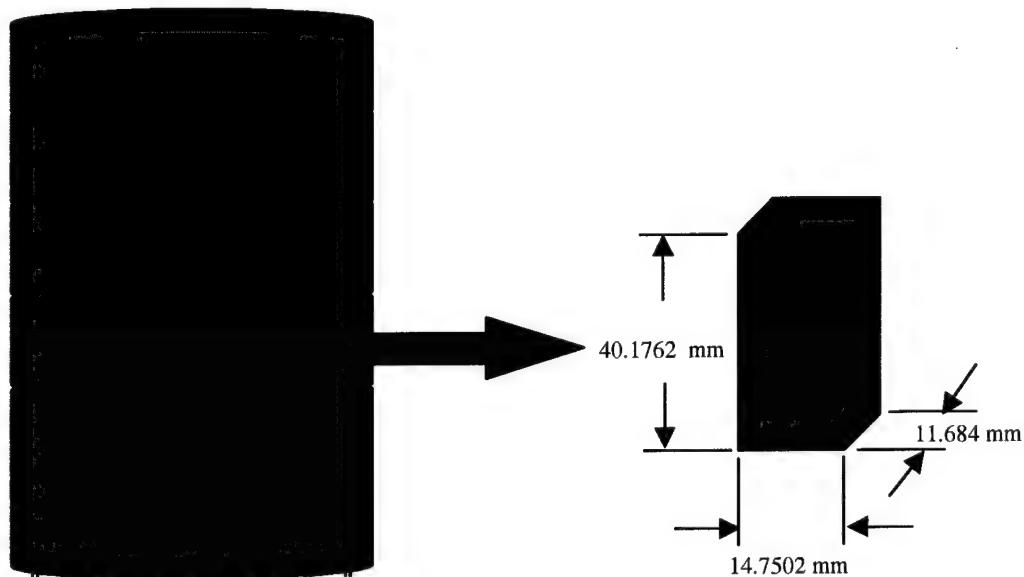


Figure 7. Dimensions of a single, undeformed fragment in the WDU-33/B warhead.

## 2. Five Inch Standoff Results

A standoff distance of five inches was selected as a lower bound for simulating WDU-33/B warheads in alignment with each other. The problem setup is illustrated in Figure 2. The donor warhead was initiated in the aft (top) center position where the fuse would be located. The position where detonation is initiated is important because it controls the fragment trajectories as shown below. For the five-inch standoff, the condition of the casing just prior to contact with the

acceptor (100 microseconds) is shown in Figure 8. The hanger assembly shown in this figure was not oriented to impact the acceptor since this would be the configuration for a wing mounted missile. As expected, the rings of free fragments around the center have the highest radial expansion speed outward. The top and bottom closure plates, along with the top and bottom rings of fragments, are maintained as a contiguous mass for a longer time since the top of these fragment rings did not have a score line.

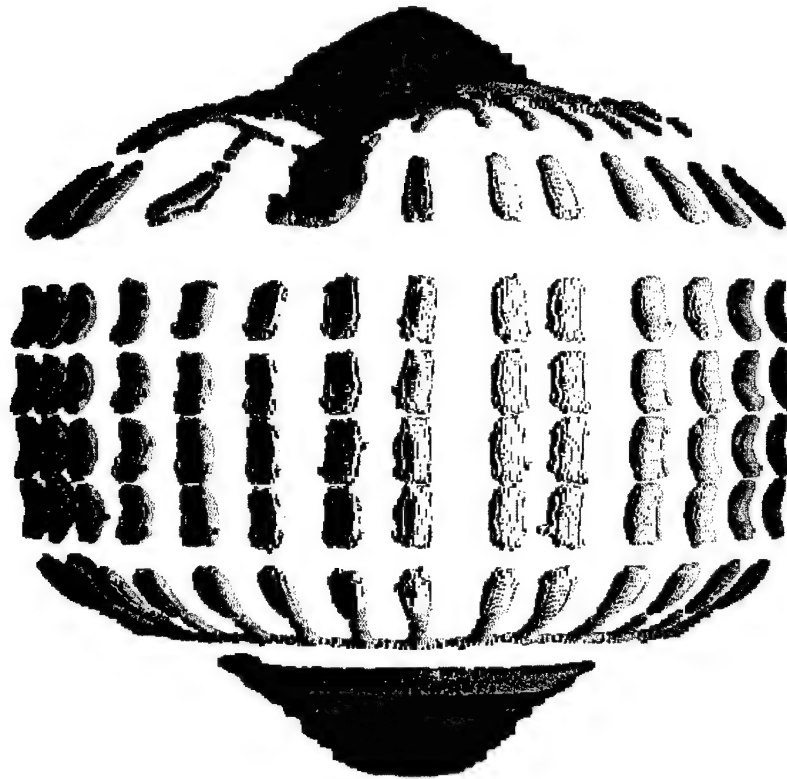


Figure 8. Early time explosive expansion of the donor warhead.

The evolution of the explosive expansion can be seen in the 2-D slice of the 3-D simulation. This is shown in Figure 9. At the time impact occurs (100 microseconds), rupture of the donor case is starting, so impact on the acceptor is closer to that of case slap. The detonation point of the donor warhead along the top center has resulted in a pressure profile that induces the center fragments to move slightly downwards. This motion becomes more obvious for the 33.5 inch standoff.

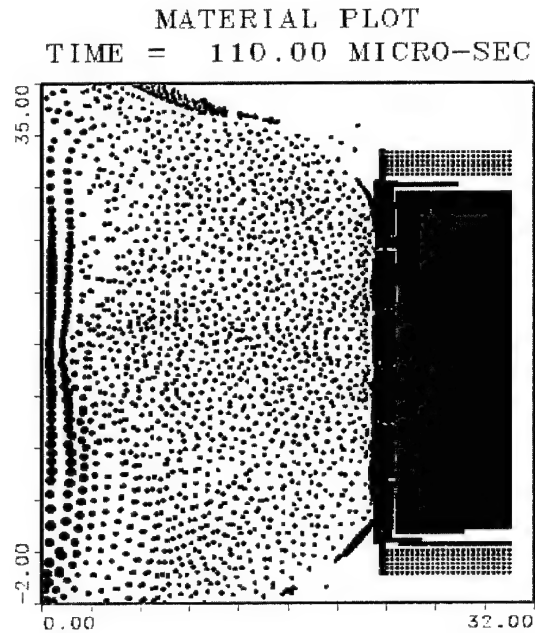
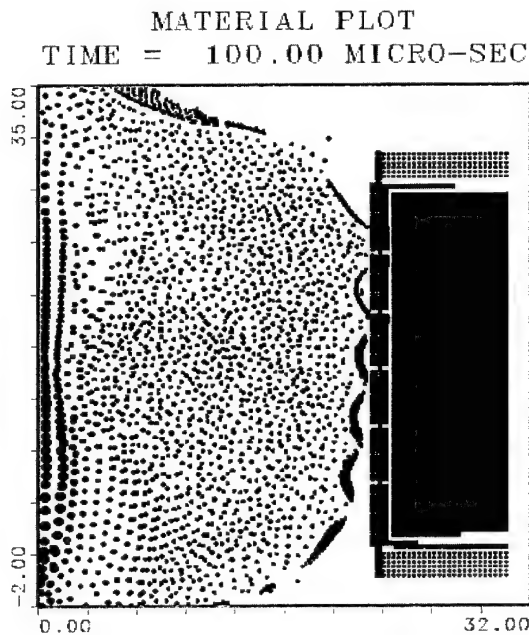


Figure 9. Two-dimensional slice showing evolution of the donor warhead expansion.

Detonation of the acceptor is underway by about 110 microseconds (Figure 10). The peak pressure is 300 kbar and is that of the detonation front in the explosive.

Figure 11 is a view from the position of the donor warhead and shows the incoming (outgoing from the view location) fragments as they approach the acceptor warhead. The view is from inside the donor warhead looking towards the acceptor. By this time, all chemical energy (30.8 MJoules) is liberated. In Figure 12, the deformation of the acceptor outer casing is shown at 120 microseconds. At this time, detonation is underway but has not had time to cause the casing to visibly expand. The expansion of the warhead casing due to detonation is clearly evident by 140 microseconds (Figure 13).

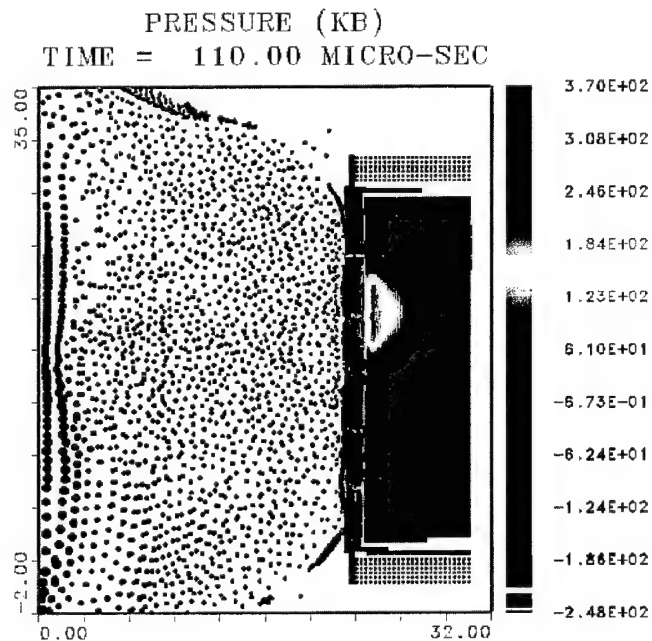


Figure 10. Pressure state of acceptor warhead at incipient detonation.

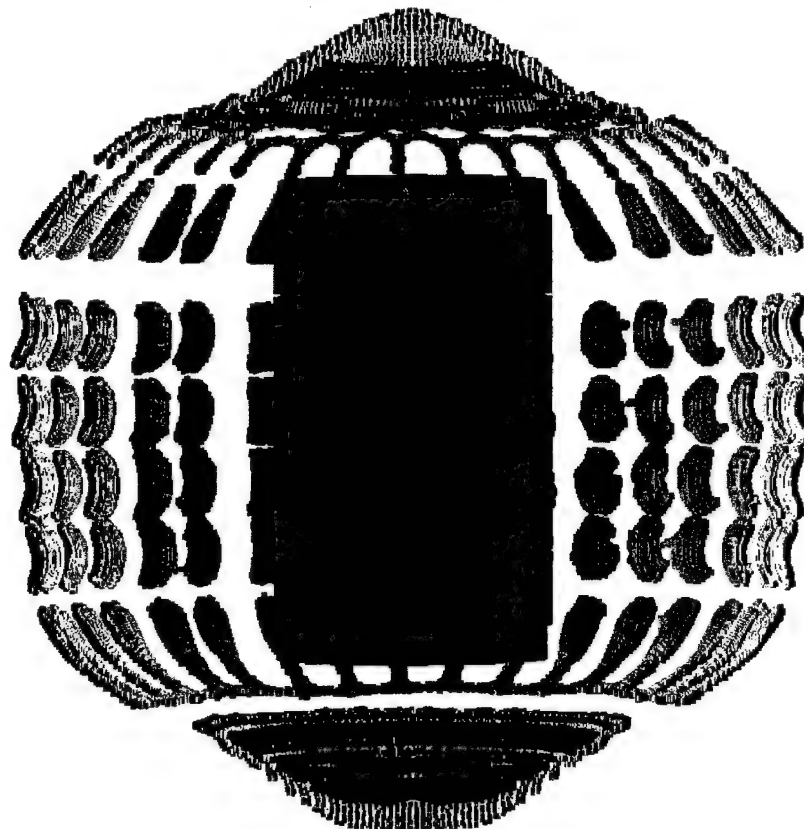


Figure 11. Case expansion shortly after impact (110 microseconds).

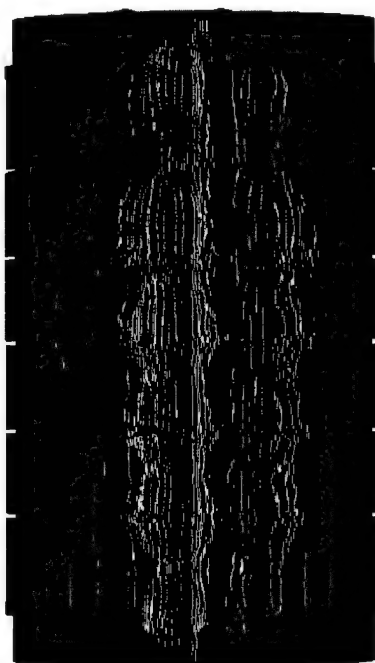


Figure 12. Acceptor casing damage for 5 inch standoff distance at 120 microseconds.



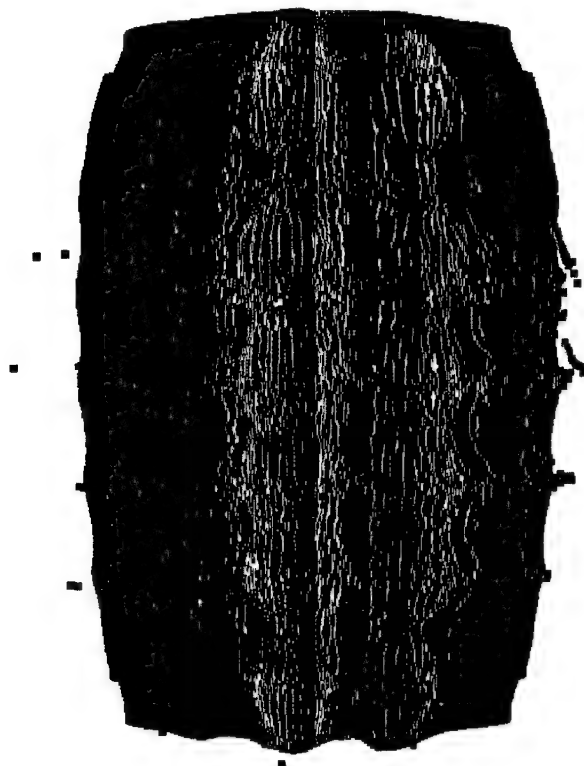


Figure 13. Acceptor casing showing explosive expansion for 5 inch standoff at 140  $\mu$ sec.

### 3. 33.5 Inch Standoff Calculation

A standoff distance of 33.5 inches was selected for this simulation with the intention of replicating the standoff distance between AIM-120 missiles in the second and third wing mounting positions (the first position being the wing tip position) of an F-16 aircraft. Hand measurements were taken from a fully loaded F-16 (Figure 14). The relative offset of the two missiles along the missile axis (measured to be about 27 inches) was not included. As noted previously, and in coordination with ongoing testing program, the warheads in these simulations were in direct alignment across each standoff distance.

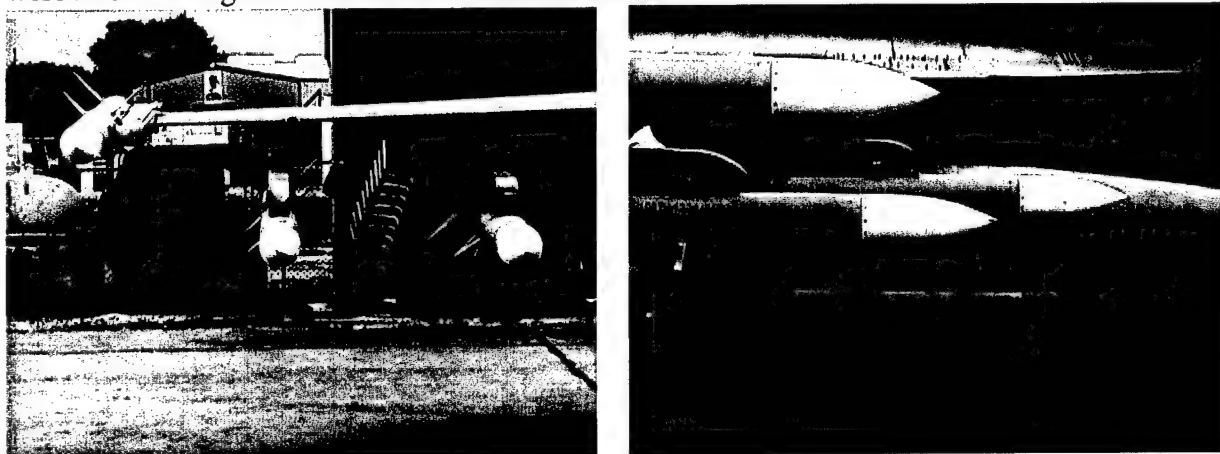


Figure 14. F-16 wing mounted AIM-120s.

The problem setup was similar to that for the previous simulation except for the standoff distance (Figure 2).

Since the hanger assembly was in the vertical upward position for both wing mounted missiles, it would not be ejected in the direction of the adjacent missile in a detonation. For this reason, it was not included in this simulation. The larger standoff distance in this simulation offered more opportunity for the fragment distribution to be affected by the initial conditions. For example, the slight downward component of velocity for the center fragments caused the lower ring of fragments to narrowly miss the acceptor (Figure 15). This 2-D slice was taken at 3.79 cm from the centerline. In this figure, the fourth fragment from the bottom disappears by 550  $\mu$ s because it moves out of the 2-D slice plane. Also resulting from the long standoff distance is the wide separation between the radially expanding fragments. By the time they impact, they have separated enough for the acceptor warhead to fit through, had the angular position of the donor been adjusted by a few degrees prior to detonation. For the initial orientation of the donor in this simulation, the resulting radial trajectory of the fragments and the final impact position is shown in Figures 16 and 17. The radial position of the fragment first to impact, and the one adjacent to it, is shown in the 2-D slice view shown in Figure 17. As seen in this figure, the initial angular position of the score marks in the donor warhead is critical to the location of impact on the acceptor warhead. A few degrees rotation in the counter-clockwise direction of the donor warhead would have produced a fragment distribution that missed the acceptor warhead.

From the pressure contours shown in Figure 18, it can be seen that detonation is initiated primarily by the shock induced by the second fragment from the bottom.

The three dimensional view of the donor fragments at impact is shown in Figures 19 and 20. In Figure 20, explosive expansion is apparent in the casing by 570 microseconds. The plastic deformation in the acceptor casing, due primarily from fragment impact, is shown in Figure 21.

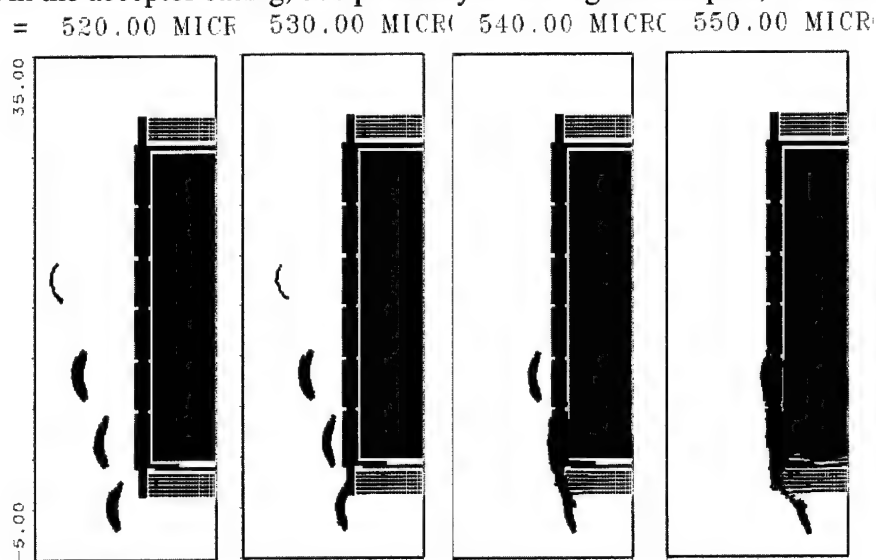


Figure 15. Progression of impacting fragments on the acceptor warhead with a 33.5 inch standoff.

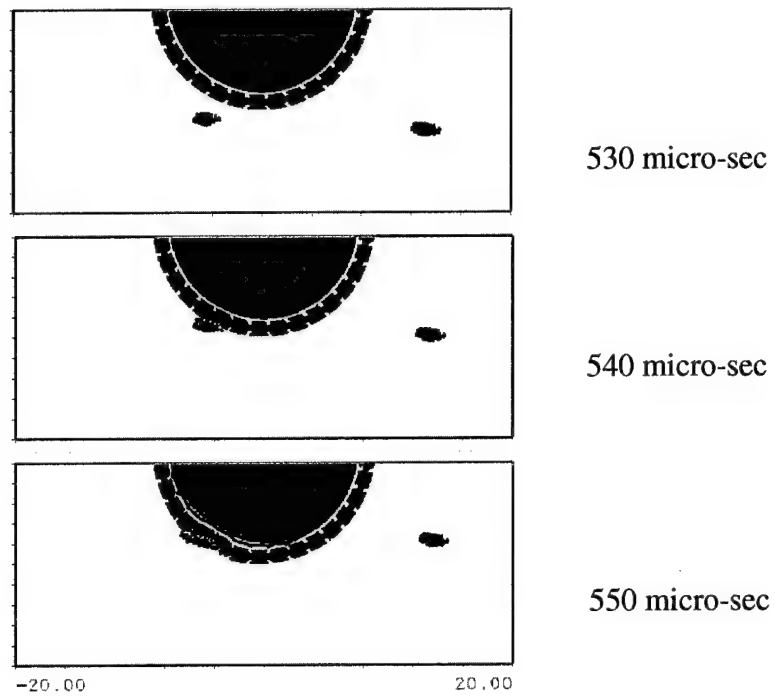


Figure 16. Radial distribution of fragments at impact for the 33.5 inch standoff.

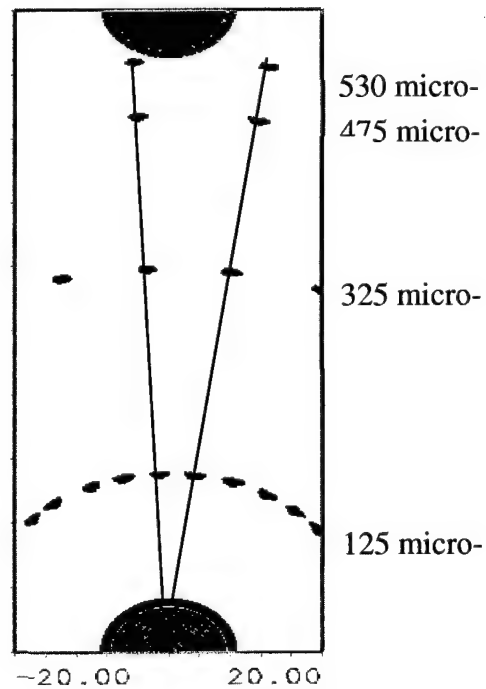


Figure 17. Fragment evolution for the 33.5 inch standoff simulation.

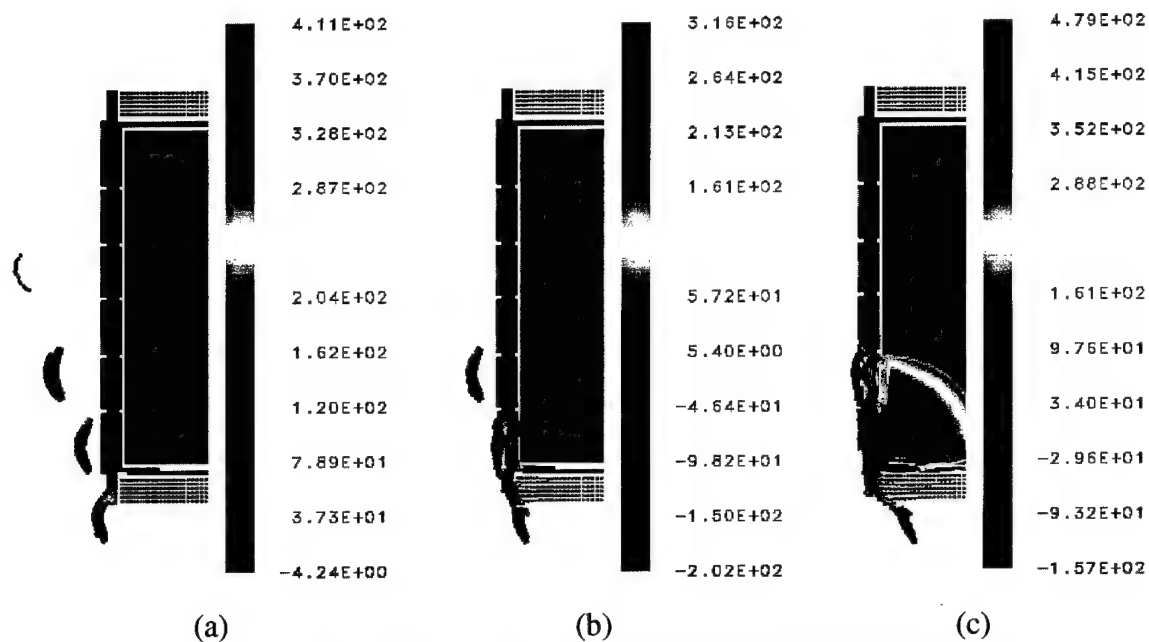


Figure 18. Pressure contours (kbar) in the acceptor warhead at (a) 530, (b) 540, and (c) 550 microseconds.



Figure 19. Acceptor warhead at 510  $\mu$ sec for a standoff distance of 33.5 inches.



Figure 20. Acceptor warhead at 570  $\mu$ sec showing explosive expansion.



Figure 21. Damage to acceptor casing at the start of induced detonation (540 microseconds).

## **Experimental Effort**

Well-controlled and highly instrumented full-scale field experiments will be conducted to assess susceptibility of the AIM-120 warhead to fragment impacts. There are two main objectives:

1. To experimentally investigate probability of fragment impact induced detonation of the AIM-120 warhead (WDU-33/B) and occurrence of Maximum Credible Event (MCE) as a function of standoff distance, and
2. To provide high fidelity fragmentation and impact data essential for calibration and validation of the analytical tools used for characterizing impact induced detonation phenomena.

A myriad of diagnostics including Time Of Arrival (TOA) pins, pressure gages, and witness plates are placed at prescribed ranges around the test bed to measure emanating shock wave velocity and pressure as well as monitoring fragments propagation. Other transducer and monitoring systems used are Photodiodes and high-speed cameras. Photodiodes are placed on the outer surface of the donor warhead to detect first light break-out of the warhead indicating warhead case rupture. The high-speed cameras will be used to record formation of the fireball.

### **1. Test Plan**

Under the auspices of the Defense Threat Assessment Agency Albuquerque Office (DTRA AO), Applied Research Associates, Inc. has developed a comprehensive test plan to conduct six AIM-120 warhead detonation tests [27]. Figures 22 through 26 illustrate specifics of these test series including test bed layouts, warhead donor/acceptor placement and the instrumentation configurations.

It should be noted that no test was done while this paper was being prepared and therefore, no correlation with the calculational prediction was performed.

## Conclusions

A novel first principle particle mechanics code (*SPH*) was used to simulate the dynamics of fragment impact induced detonation of the WDU-33/B warhead. Two distinct standoff distances of 5 and 33.5 inches were used in this simulation. An ideal configuration, where the acceptor and the donor warheads were in perfect alignment, was assumed in these calculations.

For these special ideal cases where aerodynamic effects were not included, simulation predicted acceptor warhead detonating at both standoff distances. It was shown that the likelihood of a perfectly normal fragment impact on the acceptor warhead decreases with the increasing standoff distance which consequently diminishes the likelihood of sympathetic detonation. Furthermore, fragment distribution pattern indicates that the introduction of a relative axial offset between the donor and acceptor warheads will greatly influence deposition of kinetic energy in the acceptor warhead and hence the possibility of sympathetic detonation. Exact details of these geometrical and physical phenomena will be fully explored once the experimental results become available.

Finally, as has been demonstrated, dynamics of the warheads interactions under high-strain rate-loading due to the high velocity fragment impact and all the intervening processes including warhead rupturing, fragmentation, and fragment distribution can be simulated numerically.

## References

1. C. Luehr and F.A. Allahdadi, 32<sup>nd</sup> Aerospace Sciences, AIAA 94-0066, January 1994.
2. F.A. Allahdadi and I.I. Oleinik, International Congress of Industrial and Applied Mathematics, Hamberg, Germany, June 1995.
3. L. Libersky, A. Petschek, T. Carney, J. Hipp, and F. Allahdadi, Journal of Computational Physics, Vol.109, No.1, November 1993.
4. L. Lucy and J. Astron, Vol.83, 1013, 1977.
5. R. Gingold and J. Monaghan, Mon. Not. R. Astron. Soc., 181, 375, 1977.
6. R. Gingold and J. Monaghan, J. of Comput. Physics, 46, 429, 1982.
7. J. Monaghan and R. Gingold, J. of Comput. Physics, 52, 374, 1983.
8. J. Monaghan, SIAM J. Sci Stat. Comput. 3, 422, 1982.
9. J. Monaghan, Comput. Physics Rev. 3, 71, 1985.
10. W. Benz, Numerical Modeling on Nonlinear Stellar Pulsation: Problems and Prospects, Kluwer Academics, Boston, MA, 269, 1990.
11. J. Monaghan J. of Computational Physics, 52, 374, 1983.
12. J. Monaghan, Computer Physics Reports, North Holland, Amsterdam, 71, 1985.
13. C. Truesdell and W. Noll, in Handbunch der Physik, Vol. III, Part3, Edited by S. Flugge, Springer-Verlag, Berlin, 42, 1965.
14. W. Herrmann, in Proceedings, 3rd Int. Conf. On Constitutive Laws for Engineering Materials, Tucson, AZ, 1987.
15. J. Von Neumann and R. Richtmyer, J. Appl. Physics 21, 232, 1950.
16. G. Johnson and W. Cook, "Fracture Characteristics of Three Metals Subjected to Various Strains, Strain Rates, Temperatures and Pressures," Eng. Fract. Mech., 21, 1985
17. L. Libersky and P. Randles, "Smooth Particle Hydrodynamics: Some recent improvements and applications, to be published in a special issue of Computer Methods in Applied Mechanics and Engineering entitled "Meshless Method" 1996.
18. Memo to AFRL/DEPA from the Energetic Materials Branch, Eglin Air Force Base, "JWL EOS Coefficients for AFX-108," 4 May 1998.
19. L. E. Fried, "CHEETAH 1.39 User's Manual," Lawrence Livermore National Laboratory, Livermore, CA, Report No. UCRL-MA-117541, Rev. 3, March 1996.
20. D. E. Lambert and S. A. Aubert, et. al. "Characterization of the Hydrodynamic Performance Properties of AFX-235 and 65/35 Fine Grain Octol Explosives," WL-TR-96-7035, June 1996.
21. M. Wagenhals, et al., "Sympathetic Detonation Analysis of AMRAAM Warheads in Stacked CNU-415/E Shipping Containers (U)," Naval Weapons Center, China Lake, CA, NWC-TP-7011, May 1991, Confidential Report.



22. C. L. Mader and C. A. Forest, "Two-Dimensional Homogeneous and Heterogeneous Detonation Wave Propagation," Los Alamos Scientific Laboratory, LA-6259 (U), June 1976.
23. Capt. Scott Jeffers, AFSC, contacted Mike Gunger at OTI who has done the numerical modeling for the High Explosive Research Facility (HERD).
24. T. N. Hall and J. R. Holden, "Navy Explosives Handbook", NSWC MP 88-116, October 1988
25. B. M. Dobratz and R. C. Crawford, "LLNL Explosives Handbook," UCRL-52997, Jan 1985.
26. E. A. Lundstrom, "A Numerical Study of Fragment Impact on Bare Explosive," Proceedings of the 1993 JANNAF Propulsion Systems Hazards Subcommittee Meeting, CPIA Publication 599, May 1993, pp. 273-288.
27. L. Bamert and S. Babcock, "Program Plan for Task Order (TO) 4.04/00 Explosive Safety Testing. June 11 1998.